Numerical Heat Transfer, Part A, vol. 19, pp. 65–83, 1991

NUMERICAL STUDY OF THE EFFECT OF INLET GEOMETRY ON STRATIFICATION IN THERMAL ENERGY STORAGE

Afshin J. Ghajar and Yousef H. Zurigat
School of Mechanical and Aerospace Engineering, Oklahoma State University, Stillwater, Oklahoma 74078

A finite difference computer code incorporating two methods of discretization for the advection terms in the flow governing conservation equations has been developed. These methods are the weighted upwind difference scheme (WUDS) and the second-order upwind difference scheme (SOUDS). Application of the code to a stratified thermal storage showed very good agreement between the experimental and the predicted temperature profiles when using SOUDS as opposed to WUDS. Investigation of the effect of inlet geometry on thermal stratification in a thermal storage tank was carried out using the SOUDS method. Results show that the effect of inlet geometry is negligible for Richardson numbers above 10. Thus a performance criterion for stratified thermal storage tanks with different inlet geometries has been established.

INTRODUCTION

Predictions of fluid flow and heat transfer using the finite difference method are seriously affected by numerical diffusion, instability, and computational cost. Discretization schemes based on conventional "upwind" or "donor cell" differencing of convective terms give rise to a discretization error (numerical diffusion) that limits the prediction accuracy.

Numerical diffusion (truncation and crossflow) is shown [1] to be significant in comparison with physical diffusion. As a result, thermal hydraulic computer predictions generally produce more mixing than is seen experimentally. This led to the development of several new discretization schemes for the convective terms to reduce numerical diffusion. A survey of the existing schemes was conducted [2] and suggested that the second-order upwind, the skew upwind, and the quadratic upwind interpolation difference schemes offer better accuracy than the conventional upwind scheme or its derivative, the weighted upwind difference scheme (WUDS).

In this study the second-order upwind difference scheme (SOUDS) was implemented to study the problem of mixed convection in stratified thermal energy storage. A review of this subject has been conducted in our previous studies [3, 4]. Most of the modeling studies of stratified flow in storage devices have used conventional upwind schemes for approximating the convective terms in the governing equations. In this

Y. H. Zurigat's present address is ESM Department of Virginia Polytechnic Institute and State University, Blacksburg, Virginia 24061.

Support for this research provided by the Oklahoma State University Center for Energy Research under grant 1150726 is gratefully acknowledged.

NOMENCLATURE

C_P	specific heat at constant pressure
f	friction factor in the baffle perforations
g	acceleration of gravity
H	effective height between tank inlet and outlet
k	molecular thermal conductivity
k_t	eddy conductivity
l	length scale of the resistance term
P	pressure
Q	heat flux
r	radius
R_x, R_y	resistance force components in x and y directions
Ri	Richardson number ($=\Delta\rho g H/\rho_m V^2$)
t	time
t^*	dimensionless time ($=Vt/H$)
T	temperature
u	velocity in the x or r direction
v	velocity in the y direction
V	average vertical velocity
x, y	Cartesian or cylindrical ($x \equiv r$) coordinate
α	donor cell parameter
β	coefficient of thermal expansion $\{=(\rho_0 - \rho)/[\rho_0(T - T_0)]\}$
γ	function
Δ	designates difference when used as prefix
ζ	index for Cartesian ($\zeta = 0$) or cylindrical ($\zeta = 1$) coordinate
μ	viscosity
ρ	density
ϕ	scalar dependent variable (P or T, for example)
ω	overrelaxation factor

Subscripts

b	boundary
C	center
eff	effective
E	east
i, j	indices of computational grid location
l	laminar (molecular)
m	mean
N	north
S	south
t	turbulent
u	of the u cell
v	of the v cell
W	west
x	in the x or r direction
y	in the y direction
0	initial reference state

Superscripts

n	at the previous time step
$n+1$	at the current time step
N	at the previous iteration
$N+1$	at the current iteration
T	of the T cell
P	of the P cell
v	of the v cell
u	of the u cell
ϕ	of the ϕ cell

paper the SOUDS, which was shown [2] to be superior to WUDS, is used to investigate the effect of the inlet configuration on stratification in thermal storage tanks. The inlet geometry has been shown [4] to be one of the major contributors to mixing in stratified storage. The studies [4, 5] have pointed to the existence of the limiting Richardson number, above which the effect of the inlet geometry vanishes. This criterion is significant to the designers of stratified thermal storage. In this study a two-dimensional flow model with reduced numerical diffusion is utilized to verify previous findings [4, 5], which used a one-dimensional flow model in conjunction with experiments. Based on this study, a general criterion that characterizes the influence on the inlet geometry via a limiting Richardson number has been developed.

MATHEMATICAL MODEL

The flow is governed by the well-known conservation equations of mass, momentum, and energy. In the following formulation, it is assumed that the flow is turbulent

and the viscous dissipation is negligible. Also the Boussinesq approximation is invoked, i.e., the density is assumed constant except in the buoyancy term of the y momentum equation. Then the governing equations written in primitive variables and in conservation form in both Cartesian ($\zeta = 0$) and cylindrical coordinates ($\zeta = 1, x \equiv r$) reduce to

Continuity

$$\frac{\partial u}{\partial x} + \frac{\partial v}{\partial y} + \zeta \frac{u}{x} = 0 \tag{1}$$

x and y momentum

$$\frac{\partial u}{\partial t} + \frac{\partial uu}{\partial x} + \frac{\partial uv}{\partial y} + \zeta \frac{u^2}{x} = -\frac{1}{\rho_0}\frac{\partial P}{\partial x} + \frac{\partial}{\partial x}\left(\frac{\mu_{\text{eff}}}{\rho_0}\frac{\partial u}{\partial x}\right) + \frac{\partial}{\partial y}\left(\frac{\mu_{\text{eff}}}{\rho_0}\frac{\partial u}{\partial y}\right) + \zeta\left[\frac{\mu_{\text{eff}}}{x\rho_0}\left(\frac{\partial u}{\partial x} - \frac{u}{x}\right)\right] - \frac{R_x}{\rho_0 l_x} \tag{2}$$

$$\frac{\partial v}{\partial t} + \frac{\partial uv}{\partial x} + \frac{\partial vv}{\partial y} + \zeta \frac{uv}{x} = -\frac{1}{\rho_0}\frac{\partial P}{\partial y} + g_y\beta(T - T_0) + \frac{\partial}{\partial x}\left(\frac{\mu_{\text{eff}}}{\rho_0}\frac{\partial v}{\partial x}\right) + \frac{\partial}{\partial y}\left(\frac{\mu_{\text{eff}}}{\rho_0}\frac{\partial v}{\partial y}\right) + \zeta\frac{\mu_{\text{eff}}}{x\rho_0}\frac{\partial v}{\partial x} - \frac{R_y}{\rho_0 l_y} \tag{3}$$

Energy

$$\frac{\partial T}{\partial t} + \frac{\partial uT}{\partial x} + \frac{\partial vT}{\partial y} + \frac{\zeta}{x}uT = \frac{\partial}{\partial x}\left(\frac{k_{\text{eff}}}{\rho_0 C_P}\frac{\partial T}{\partial x}\right) + \frac{\partial}{\partial y}\left(\frac{k_{\text{eff}}}{\rho_0 C_P}\frac{\partial T}{\partial y}\right) + \zeta\frac{k_{\text{eff}}}{x\rho_0 C_P}\frac{\partial T}{\partial x} \tag{4}$$

The effective viscosity and conductivity appearing in the governing equations are defined as the sum of the laminar and turbulent contributions, that is,

$$\mu_{\text{eff}} = \mu_{\text{l}} + \mu_{\text{t}} \tag{5}$$

$$k_{\text{eff}} = k_{\text{l}} + k_{\text{t}} \tag{6}$$

where μ_{t} and k_{t} are the turbulent contributions obtained from a suitable turbulence model.

The resistance terms R_x and R_y arise due to the presence of solid or perforated obstructions in the flow field as defined by Sha et al. [6]:

$$R_x = \frac{1}{2} f\rho |u| u \tag{7}$$

$$R_y = \frac{1}{2} f\rho |v| v \tag{8}$$

where the friction factor f is to be calculated based on the diameter and thickness of the perforations. The l_x and l_y appearing in the resistance terms are the appropriate length scales associated with R_x and R_y, respectively. They may be taken as the grid sizes in the x and y directions.

FINITE DIFFERENCE FORMULATION

Grid System

The two-dimensional plane or axisymmetric flow domain is divided into rectangular cell divisions with nonuniform spacing (see Fig. 1). The location of the field variables P, u, v, and T are shown for an arbitrary i, j cell. It is seen that P and T are cell centered, while the u and v velocities are located on the faces of the cell.

This staggered arrangement gives rise to three different control volumes, the u cell, the v cell, and the $\phi(P, T)$ cell for solving the x (or r) momentum, the y momentum, and the scalar transport equations, respectively. With this convention the following

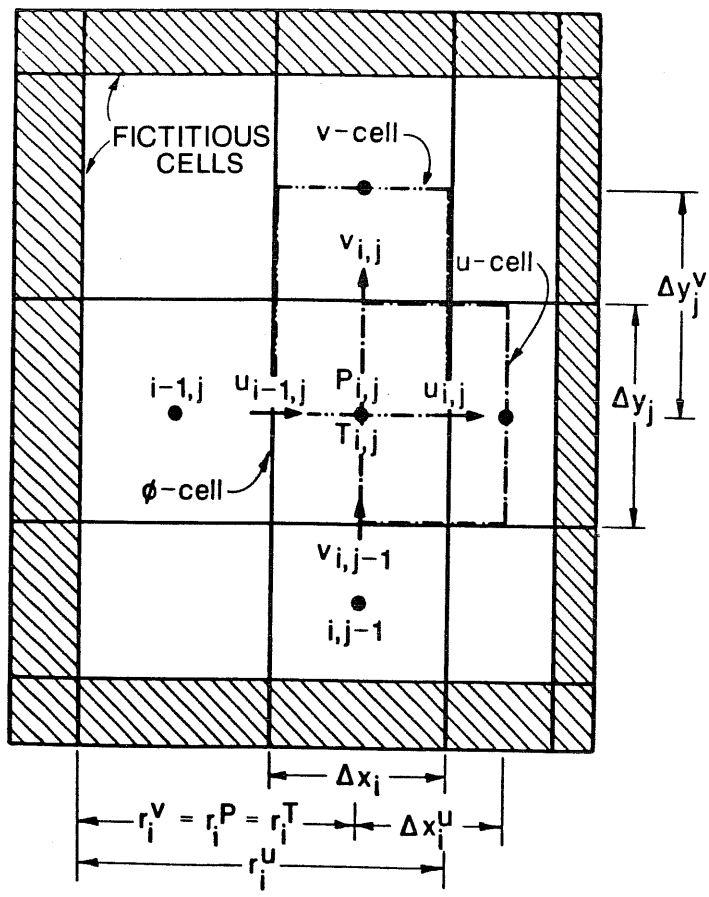

Fig. 1 Grid layout showing location of the nodal variables u, v, P, and T, (i, j) notation, and the $\phi(T, P)$, u, and v cells.

grid dimensions are defined:

$$\Delta xh_i = \frac{\Delta x_i}{2} \tag{9}$$

$$\Delta yh_j = \frac{\Delta y_j}{2} \tag{10}$$

$$\Delta x_i^u = \Delta xh_i + \Delta xh_{i+1} \tag{11}$$

$$\Delta y_j^v = \Delta yh_j + \Delta yh_{j+1} \tag{12}$$

where Δx_i and Δy_i are the ϕ cell dimensions. In addition, in the axisymmetric cylindrical coordinates the following dimensions are defined:

Radius to the center of the u cell

$$r_i^u = \sum_{n=2}^{i} \Delta x_n \tag{13}$$

Radius to the center of the v and ϕ cells

$$r_i^v = r_i^\phi = r_i^u - \Delta xh_i \tag{14}$$

where r_i^ϕ stands for r_i^T or r_i^P.

The computational domain is surrounded by a layer of fictitious cells on all sides to allow for enforcing the hydrodynamic and thermal boundary conditions.

Discretized Equations

The approximation of the advection terms requires special treatment, which, as pointed out in the introduction, has been the topic of numerous studies. The explicit formulation [7] for discretizing the conservation equations in Cartesian coordinates is adopted and extended to axisymmetric cylindrical coordinates. In this paper, only the continuity and x momentum equations are discretized in detail. The detailed discretization of the rest of the governing equations is described in Ref. [8].

Continuity equation

$$\frac{u_{i,j}^{n+1} - u_{i-1,j}^{n+1}}{\Delta x_i} + \frac{v_{i,j}^{n+1} - v_{i,j-1}^{n+1}}{\Delta y_j} + \frac{\zeta(u_{i,j}^{n+1} + u_{i-1,j}^{n+1})}{2r_i^\phi} = D_{i,j}^{n+1} \tag{15}$$

where the superscript $n + 1$ indicates the values at the new time step. The velocity divergence, $D_{i,j}^{n+1}$, should equal zero for perfect satisfaction of continuity. However, this is difficult to achieve numerically, and some vanishingly small mass residue in a given computational cell is allowed within a preset tolerance. The satisfaction of continuity in this manner serves in solving the pressure-velocity coupling problem discussed later.

x momentum equation

$$\left(\frac{\partial u}{\partial t}\right)_{i,j} = \frac{u_{i,j}^{n+1} - u_{i,j}^{n}}{\Delta t} \tag{16}$$

where the superscript n indicates the value at previous time step.

$$\left(\frac{\partial uu}{\partial x}\right)_{i,j} = \text{DUUDX} = \frac{u_{\text{E,u}}\tilde{u}_{\text{E}} - u_{\text{W,u}}\tilde{u}_{\text{W}}}{\Delta x_i^u} \tag{17}$$

$$\left(\frac{\partial vu}{\partial x}\right)_{i,j} = \text{DVUDX} = \frac{v_{\text{N,u}}\tilde{u}_{\text{N}} - v_{\text{S,u}}\tilde{u}_{\text{S}}}{\Delta y_j} \tag{18}$$

$$\left(\frac{\zeta uu}{x}\right)_{i,j} = \text{FUU} = \frac{\zeta(u_{\text{E,u}}\tilde{u}_{\text{E}}\,\Delta xh_i + u_{\text{W,u}}\tilde{u}_{\text{W}}\,\Delta xh_{i+1})}{r_i^u\,\Delta x_i^u} \tag{19}$$

$$\left(\frac{\partial P}{\partial x}\right)_{i,j} = \text{DPDX} = \frac{P_{i+1,j}^{n} - P_{i,j}^{n}}{\Delta x_i^u} \tag{20}$$

$$\frac{\partial}{\partial x}\left(\mu_{\text{eff}}\frac{\partial u}{\partial x}\right)_{i,j} = \text{VISXU} = \left[\mu_{\text{eff(E,u)}}\frac{u_{i+1,j}^{n} - u_{i,j}^{n}}{\Delta x_{i+1}} - \mu_{\text{eff(W,u)}}\frac{u_{i,j}^{n} - u_{i-1,j}^{n}}{\Delta x_i}\right]\Big/\Delta x_i^u \tag{21}$$

$$\frac{\partial}{\partial y}\left(\mu_{\text{eff}}\frac{\partial u}{\partial y}\right)_{i,j} = \text{VISYU} = \left[\mu_{\text{eff(N,u)}}\frac{u_{i,j+1}^{n} - u_{i,j}^{n}}{\Delta y_j^v} - \mu_{\text{eff(S,u)}}\frac{u_{i,j}^{n} - u_{i,j-1}^{n}}{\Delta y_{j-1}^v}\right]\Big/\Delta y_j \tag{22}$$

$$\zeta\frac{\mu_{\text{eff}}}{x}\left(\frac{\partial u}{\partial x} - \frac{u}{x}\right)_{i,j} = \text{VISCU} = \zeta\mu_{\text{eff(C,u)}}\left[\frac{u_{i+1,j}^{n} - u_{i-1,j}^{n}}{2\Delta x_i^u} - \frac{u_{i,j}}{r_i^u}\right]\Big/r_i^u \tag{23}$$

where

$$\mu_{\text{eff(E,u)}} = \mu_{\text{eff}(i+1,j)} \tag{24}$$

$$\mu_{\text{eff(W,u)}} = \mu_{\text{eff}(i,j)} \tag{25}$$

$$\begin{aligned}\mu_{\text{eff(N,u)}} = {} & [(\mu_{\text{eff}(i+1,j+1)}\,\Delta xh_i + \mu_{\text{eff}(i,j+1)}\,\Delta xh_{i+1})\,\Delta yh_j \\ & + (\mu_{\text{eff}(i+1,j)}\,\Delta xh_i + \mu_{\text{eff}(i,j)}\,\Delta xh_{i+1})\,\Delta yh_{j+1}]/(\Delta x_i^u\,\Delta y_j^v)\end{aligned} \tag{26}$$

$$\begin{aligned}\mu_{\text{eff(S,u)}} = {} & [(\mu_{\text{eff}(i+1,j)}\,\Delta xh_i + \mu_{\text{eff}(i,j)}\,\Delta xh_{i+1})\,\Delta yh_{j-1} \\ & + (\mu_{\text{eff}(i+1,j-1)}\,\Delta xh_i + \mu_{\text{eff}(i,j-1)}\,\Delta xh_{i+1})\,\Delta yh_j]/(\Delta x_i^u\,\Delta y_{j-1}^v)\end{aligned} \tag{27}$$

$$\mu_{\text{eff(C,u)}} = [\mu_{\text{eff}(i+1,j)}\,\Delta xh_i + \mu_{\text{eff}(i,j)}\,\Delta xh_{i+1}]/\Delta x_i^u \tag{28}$$

The tilde is used throughout this paper to designate the velocity terms that are derived differently for the WUDS and SOUDS methods (see Refs. [2] and [8]). Also, the subscripted velocities in Eqs. (17)–(19) are the velocities at the corresponding sides of the u cell. Thus, $u_{E,u}$ designates the u velocity at the eastern side of the u cell.

The finite difference analog of the resistance term in Eq. (2) is derived by linearizing $R^{n+1}_{x(i,j)}$ as [6]

$$R^{n+1}_{x(i,j)} = A^{n}_{x(i,j)} + B^{n}_{x(i,j)}\, u^{n+1}_{i,j} \tag{29}$$

where the coefficients $A^{n}_{x(i,j)}$ and $B^{n}_{x(i,j)}$ for solid baffles are defined as

$$A^{n}_{x(i,j)} = 0 \qquad B^{n}_{x(i,j)} = 10^{30} \tag{30}$$

and for perforated baffles, from Eq. (7), are

$$A^{n}_{x(i,j)} = -\frac{1}{2} f \rho^{u}_{i,j} |u^{n}_{i,j}| u^{n}_{i,j} \tag{31}$$

$$B^{n}_{x(i,j)} = f \rho^{u}_{i,j} |u^{n}_{i,j}| \tag{32}$$

where the friction factor f is a function of the baffle thickness to hole diameter ratio and the porosity of the baffle [9]. In the absence of baffles, both $A^{n}_{x(i,j)}$ and $B^{n}_{x(i,j)}$ are set to zero. The density $\rho^{u}_{i,j}$ is evaluated by

$$\rho^{u}_{i,j} = \frac{\Delta x h_{i+1} \rho^{n}_{i,j} + \Delta x h_i \rho^{n}_{i+1,j}}{\Delta x^{u}_{i}} \tag{33}$$

Substituting Eqs. (16)–(23) and (29) in Eq. (2) and rearranging explicitly gives the velocity at the new time step:

$$u^{n+1}_{i,j} = \left[u^{n}_{i,j} + \Delta t \left(-\frac{\mathrm{DPDX}}{\rho_0} + \frac{\mathrm{VISXU} + \mathrm{VISYU} + \mathrm{VISCU}}{\rho_0} - \mathrm{DUUDX} - \mathrm{DVUDX} - \mathrm{FUU} - A_{x(i,j)} \right) \right] \Big/ B_{x(i,j)} \tag{34}$$

where

$$A_{x(i,j)} = \frac{A^{n}_{x(i,j)}}{\rho_0 \, \Delta x^{u}_{i}} \tag{35}$$

$$B_{x(i,j)} = 1.0 + \frac{\Delta t B^{n}_{x(i,j)}}{\rho_0 \, \Delta x^{u}_{i}} \tag{36}$$

Notice that in the presence of nonperforated baffles, $B^n_{x(i,j)}$ evaluated by Eq. (36) is large enough [see Eq. (30)] to force the calculated velocity, Eq. (34), to vanish. When no baffles are present, $B_{x(i,j)}$ becomes unity and $A^n_{x(i,j)}$ is set to zero. When baffles are present, the calculated velocity is reduced according to the resistance encountered. The vertical baffle at the i, j location is placed such that it coincides with the right face of the ϕ cell. Finite difference equations were derived for the y momentum and energy equations (see Ref. [8]).

The finite difference analog of the resistance term in Eq. (3) is derived in a manner similar to that in Eqs. (29)–(36) with subscript x replaced by y and u velocity replaced by v velocity:

$$A_{y(i,j)} = \frac{A^n_{y(i,j)}}{\rho_0 \, \Delta y^{\mathrm{v}}_j} \tag{37}$$

$$B_{y(i,j)} = 1.0 + \frac{\Delta t B^n_{y(i,j)}}{\rho_0 \, \Delta y^{\mathrm{v}}_j} \tag{38}$$

Also the density, $\rho^{\mathrm{u}}_{i,j}$, is replaced by $\rho^{\mathrm{v}}_{i,j}$, which is evaluated as

$$\rho^{v}_{i,j} = \frac{\Delta y h_{j+1} \rho^n_{i,j} + \Delta y h_j \rho^n_{i,j+1}}{\Delta y^{\mathrm{v}}_j} \tag{39}$$

The horizontal baffle at the i, j location is situated such that it coincides with the northern face of the ϕ cell.

Equation (34) and the analogous equations for y momentum and energy, along with Eq. (15), constitute the complete finite difference analog of the conservation equations, Eqs. (1)–(4). Note that the pressure appears in both the x and y momentum equations. This velocity-pressure coupling requires special treatment, since the accuracy of the computed pressure field determines that of the computed velocity field, which in turn determines the satisfaction of continuity requirements. Thus for a given initial guess of the pressure field or for that calculated from a previous time step, the calculated velocity field will not, in general, satisfy the continuity equation, Eq. (15). An iterative adjustment of the pressure at each computational cell and the velocities thereafter is needed; this is discussed in the next section.

Pressure-Velocity Adjustment Equations

The pressure adjustment is done such that the residue $D^{n+1}_{i,j}$ in Eq. (15) is minimized. The Newton-Raphson scheme, which is iterative in character, is used to find the necessary pressure adjustment increment. The increment in the independent variable ξ that satisfies the function γ is determined from [10]:

$$\frac{\partial \gamma}{\partial \xi} \Delta \xi = -\omega \gamma \tag{40}$$

where ω is an overrelaxation factor used to speed up the convergence. Applying this to

our case and rearranging gives the correction increment in pressure:

$$\Delta P_{i,j}^{N} = -\omega D_{i,j}^{N} \Big/ \frac{\partial D_{i,j}^{N}}{\partial P_{i,j}^{N}} \tag{41}$$

where the superscript N indicates the Nth iteration in the same time step.

The new pressure is then determined by

$$P_{i,j}^{N+1} = P_{i,j}^{N} + \Delta P_{i,j}^{N} \tag{42}$$

where $P_{i,j}^{N}$ is the pressure from a previous iteration in the same time step. The pressure increment results in a velocity increment, which is obtained by writing the discretized momentum equations, for the four velocities of the ϕ cell with the new pressure, $P_{i,j}^{N+1}$, and subtracting a similar expression with $P_{i,j}^{N}$. Thus from Eq. (34) we have

$$u_{i,j}^{P(N)} = \left[u_{i,j}^{N} + \Delta t \left(\frac{P_{i,j}^{N} - P_{i+1,j}^{N}}{\rho_0 \, \Delta x_i^{u}} + \mathrm{OT} \right) \right] \Big/ B_{x(i,j)} \tag{43}$$

$$u_{i,j}^{P(N+1)} = \left[u_{i,j}^{N} + \Delta t \left(\frac{P_{i,j}^{N+1} - P_{i+1,j}^{N}}{\rho_0 \, \Delta x_i^{u}} + \mathrm{OT} \right) \right] \Big/ B_{x(i,j)} \tag{44}$$

where OT designates other terms appearing in Eq. (34). Subtracting Eq. (43) from Eq. (44) gives

$$\Delta u_{i,j}^{N+1} = u_{i,j}^{P(N+1)} - u_{i,j}^{P(N)} = \frac{\Delta t (P_{i,j}^{N+1} - P_{i,j}^{N})}{B_{x(i,j)} \rho_0 \, \Delta x_i^{u}} \tag{45}$$

or by Eq. (42), we have

$$\Delta u_{i,j}^{N+1} = \frac{\Delta t \, \Delta P_{i,j}^{N}}{B_{x(i,j)} \rho_0 \, \Delta x_i^{u}} \tag{46}$$

The new velocity $u_{i,j}^{N+1}$ is then calculated from

$$u_{i,j}^{N+1} = u_{i,j}^{N} + \Delta u_{i,j}^{N+1} = u_{i,j}^{N} + \frac{\Delta t \, \Delta P_{i,j}^{N}}{B_{x(i,j)} \rho_0 \, \Delta x_i^{u}} \tag{47}$$

In a similar fashion, we have for the velocity at the left face of the ϕ cell, $u_{i-1,j}^{N+1}$:

$$u_{i-1,j}^{N+1} = u_{i-1,j}^{N} - \frac{\Delta t \, \Delta P_{i,j}^{N}}{B_{x(i-1,j)} \rho_0 \, \Delta x_{i-1}^{u}} \tag{48}$$

The v velocities $v_{i,j}^{N+1}$ and $v_{i,j-1}^{N+1}$ are derived similarly, the result being

$$v_{i,j}^{N+1} = v_{i,j}^{N} + \frac{\Delta t\, \Delta P_{i,j}^{N}}{B_{y(i,j)} \rho_0\, \Delta y_j^{v}} \tag{49}$$

$$v_{i,j-1}^{N+1} = v_{i,j-1}^{N} - \frac{\Delta t\, \Delta P_{i,j}^{N}}{B_{y(i,j-1)} \rho_0\, \Delta y_{j-1}^{v}} \tag{50}$$

The pressure increment $\Delta P_{i,j}^{N}$ is calculated by Eq. (41), where the partial derivative is derived as follows.

Expressing the velocities on the ϕ cell faces, $u_{i,j}^{p(N)}$, $u_{i-1,j}^{p(N)}$, $v_{i,j}^{p(N)}$, and $v_{i,j-1}^{p(N)}$ [as in Eq. (43)], substituting in the continuity equation, Eq. (15), and taking the partial derivative with respect to $P_{i,j}^{N}$ gives, after some rearrangement,

$$\frac{\partial D_{i,j}^{N}}{\partial P_{i,j}^{N}} = \frac{\Delta t}{\rho_0}\left[\frac{1}{\Delta x_i}\left(\frac{1}{\Delta x_i^{u} B_{x(i,j)}} + \frac{1}{\Delta x_{i-1}^{u} B_{x(i-1,j)}}\right) + \frac{1}{\Delta y_j}\left(\frac{1}{\Delta y_j^{v} B_{y(i,j)}} + \frac{1}{\Delta y_{j-1}^{v} B_{y(i,j-1)}}\right) + \frac{\zeta}{2r_i^{P}}\left(\frac{1}{\Delta x_i^{u} B_{x(i,j)}} - \frac{1}{\Delta x_{i-1,j}^{u} x(i-1,j)}\right)\right] \tag{51}$$

Note that if baffles are absent and uniform grid spacing ($\Delta x_i = \Delta x$; $\Delta y_j = \Delta y$) is used, Eq. (51) becomes

$$\frac{\partial D_{i,j}^{N}}{\partial P_{i,j}^{N}} = \frac{2\Delta t}{\rho_0}\left[\frac{1}{\Delta x^2} + \frac{1}{\Delta y^2}\right] \tag{52}$$

Substitution of Eq. (51) in Eq. (41) results in the general pressure adjustment increment equation.

Pressure-Velocity Adjustment Iteration Procedure

The velocities calculated from the discretized equations do not, in general, satisfy the continuity requirements. The pressure and velocities are adjusted iteratively in the following order:

1. Velocities calculated from the discretized equations are used to calculate the residual $D_{i,j}^{N}$ from the continuity equation, Eq. (15).
2. The pressure adjustment increment is calculated from Eq. (41).
3. The pressure is adjusted using Eq. (42).
4. The velocities are adjusted using Eqs. (47)-(50).

These steps are repeated for each computational cell in the flow domain, keeping track of the maximum value of $D_{i,j}^{N}$ occurring during each sweep. The process of sweeping the computational domain in the above manner continues until the absolute value of the divergence $D_{i,j}^{N}$ becomes vanishingly small, i.e., $D_{i,j}^{N} < \epsilon$, where ϵ is a prescribed

tolerance, say, $\epsilon = 10^{-6}$. Boundary conditions are applied at the beginning of each iteration of the above procedure.

Boundary Conditions

No-slip, free-slip, inflow, and outflow boundary conditions are imposed as appropriate (see Ref. [11]). The thermal boundary conditions are described in detail herein. Due to the staggered grid, the imposition of boundary conditions on temperature or heat flux is not straightforward. Expressions have to be derived for the diffusion terms for the internal cells adjacent to the boundary (fictitious) cells. This is demonstrated below for a left boundary. In this case, only the x (or r) diffusion terms are involved.

Referring to Fig. 2, we have

$$\frac{\partial}{\partial x}\left(k_{\text{eff}}\frac{\partial T}{\partial x}\right)_{2,j} = \left[\left(k_{\text{eff}}\frac{\partial T}{\partial x}\right)_{\text{E}} - \left(k_{\text{eff}}\frac{\partial T}{\partial x}\right)_{\text{W}}\right]\Big/\frac{3\Delta x_2}{4}$$

$$= \left[k_{\text{eff(E)}}\frac{T_{3,j} - T_{2,j}}{\Delta x_2^u} - k_{\text{eff(W)}}\frac{T_{2,j} - T_{\text{b},j}}{\Delta x h_2}\right]\Big/\frac{3\Delta x_2}{4} \tag{53}$$

where

$$k_{\text{eff(E)}} = \frac{k_{\text{eff}(3,j)}\,\Delta x h_2 + k_{\text{eff}(2,j)}\,\Delta x h_3}{\Delta x_2^u} \tag{54}$$

$$k_{\text{eff(W)}} = \frac{k_{\text{eff}(2,j)} + k_{\text{eff}(b,j)}}{2} \tag{55}$$

Also

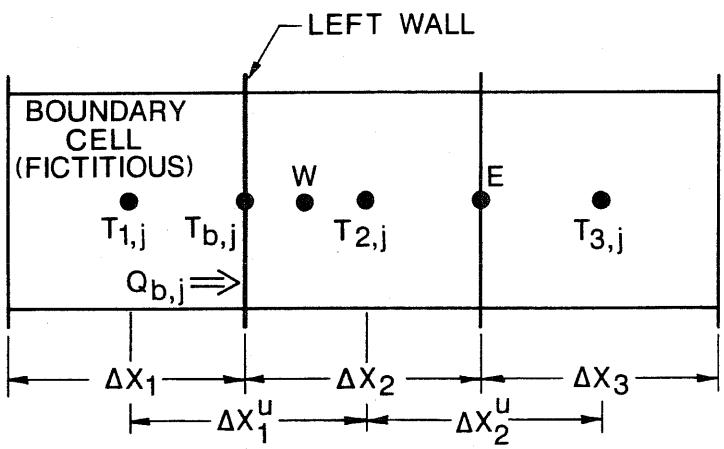

Fig. 2 Left boundary cell arrangement.

$$\left(\zeta \frac{k_{\text{eff}}}{x} \frac{\partial T}{\partial x}\right)_{2,j} = \zeta k_{\text{eff}(2,j)} \left[\frac{T_{3,j}\,\Delta x h_2 + T_{2,j}\,\Delta x h_3}{\Delta x_2^{\text{u}}} - \frac{T_{2,j} + T_{b,j}}{2} \right] \Big/ \frac{3\Delta x_2 r_2^T}{4} \tag{56}$$

where $k_{\text{eff}(b,j)}$ is calculated at $T_{b,j}$, which is stored (codewise) at $T_{1,j}$ location and

$$x_{2,j} = r_2^T \tag{57}$$

Analogous expressions for the rest of the boundaries are derived similarly. With these expressions implemented at the boundaries, the following boundary conditions demonstrated for the left wall can be imposed:

Uniform constant wall temperature

$$T_{1,j} = C \qquad \text{for all } j \tag{58a}$$

where C is the assigned temperature.

Nonuniform constant wall temperature

$$T_{1,j} = C_j \tag{58b}$$

Uniform transient wall temperature

$$T_{1,j} = C(t) \qquad \text{for all } j \tag{58c}$$

Nonuniform transient wall temperature

$$T_{1,j} = C_j(t) \tag{58d}$$

The heat flux at the wall is assigned as desired, that is, uniform or nonuniform, transient or constant. Then the wall temperature is calculated by

$$T_{\text{b},j} = T_{2,j} + Q_{\text{b},j} \frac{\Delta \tilde{x}}{k_{\text{eff(W)}}} \tag{59}$$

where $\Delta \tilde{x}$ is the diffusion length, which is equal to half of the dimension of the internal cell adjacent to the boundary, i.e., $\Delta x_2/2$. $Q_{\text{b},j}$ is the heat flux at the boundary. Thus $T_{\text{b},j}$ will vary according to the variation in $Q_{\text{b},j}$, which can be assigned for the left boundary as follows:

Uniform constant wall heat flux

$$Q_{1,j} = C \qquad \text{for all } j \tag{60a}$$

Nonuniform constant wall heat flux

$$Q_{1,j} = C_j \tag{60b}$$

Uniform transient wall heat flux

$$Q_{1,j} = C(t) \qquad \text{for all } j \tag{60c}$$

Nonuniform transient wall heat flux

$$Q_{1,j} = C_j(t) \tag{60d}$$

The insulated boundary is specified by setting the derivative across the boundary to zero. Also in the plane of symmetry the derivative across the plane should vanish. For a left insulated wall or left plane of symmetry, we have

$$T_{1,j} = T_{2,j} \qquad \text{for all } j \tag{61}$$

RESULTS AND DISCUSSION

The computer code developed based on the above formulation was first tested by application to simple flow problems with known analytical solutions. The results indicate that the performance of SOUDS is much better than WUDS (see Ref. [2]). Application of the computer code to thermocline thermal storage (constant inlet temperature) shows the same trend. Figure 3 shows the predictions compared with the experiments. The agreement between the predictions using SOUDS and the experiments is satisfactory. A high level of numerical diffusion is seen to result when using WUDS. Figure 4 confirms this trend. Based on these results, the SOUDS was used throughout the rest of this study.

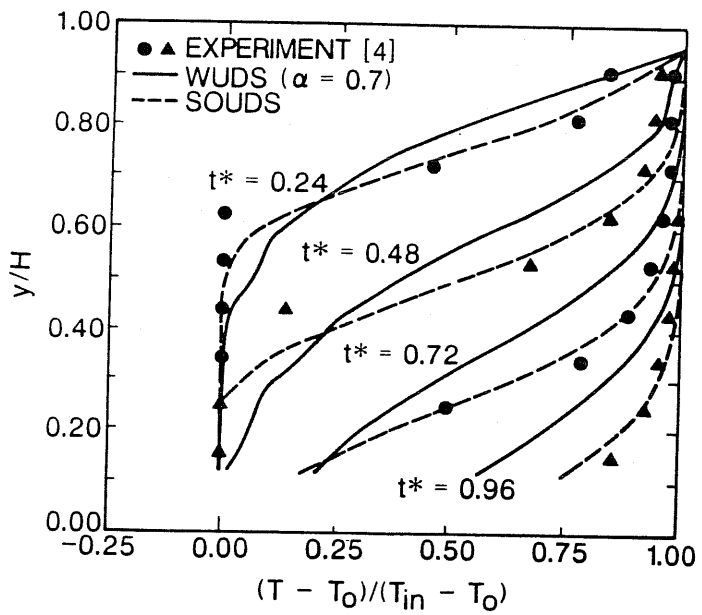

Fig. 3 Predictions of temperature profiles at the centerline in thermocline cylindrical thermal storage tank comparing SOUDS, WUDS ($\alpha = 0.7$), and the experiments of Ref. [4].

The SOUDS was first applied to the perforated inlet [4]. Figure 5 shows that a good agreement with the experiments was achieved. In this case, the conditions of the experiments were closely matched. Laminar flow was assumed in the simulation. The predictions with turbulent flow assumption (using mixing length model of Ref. [6]) showed negligible difference, indicating laminar flow under the conditions considered.

The inlet geometry has a significant effect on thermocline development in the storage tank [4]. In the early studies [4, 5] it was found that there exists a limiting Richardson number above which the inlet geometry becomes less important to thermal stratification in the thermal storage tank. Richardson number values of 3.6 [4] and 5 [5] were deduced. These findings were based on a one-dimensional flow model in which a mixing index was introduced to account for departures from one-dimensional flow behavior. With the two-dimensional model developed in this study, it is of interest to verify the above-mentioned findings.

Two inlet geometries were used in the simulations. The first was a circular disk of diameter 2.54 cm (1.0 inch) displaced 1.27 cm (0.5 inch) from the inlet pipe, which was located at the center of the top of the tank (tank dimensions are those used in Ref. [4]). For reference purposes this inlet geometry will be referred to as a solid disk diffuser. The second geometry was formed by adding to the solid disk diffuser a perforated extension that spanned the rest of the tank cross-sectional area. This geometry will be referred to as a perforated diffuser.

Simulations for the charge mode of operation (hot water pumped through the top and cold water discharged through the bottom) were conducted with the above-mentioned inlet geometries for several values of Richardson number. An insulated wall was assumed in these simulations. The Richardson number was varied by varying the

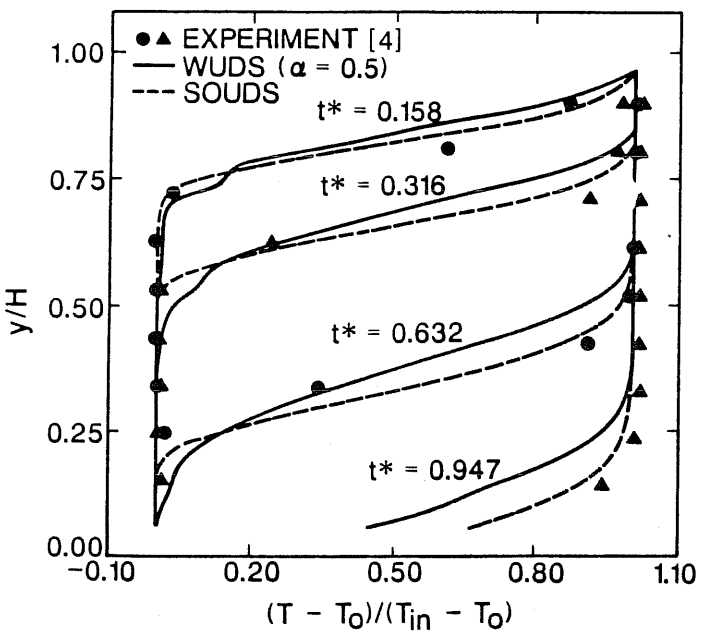

Fig. 4 Predictions of temperature profiles at the centerline in thermocline cylindrical thermal storage tank comparing SOUDS, WUDS (α = 0.5), and the experiments of Ref. [4].

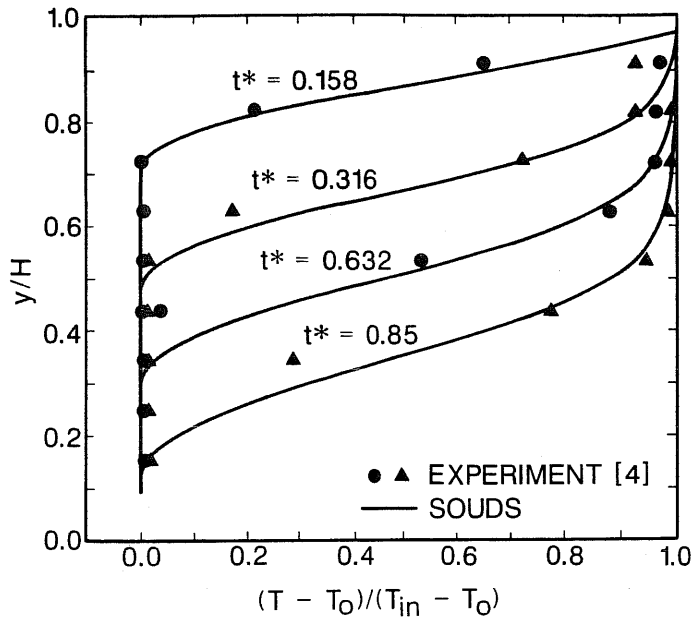

Fig. 5 Predictions of temperature profiles at the centerline in thermocline cylindrical thermal storage tank comparing SOUDS and the experiments of Ref. [4].

difference between the inlet and the initial water temperatures while maintaining the same flow rate. Figures 6*a*–6*e* show the predictions of thermocline in the storage tank as it passes through different elevations close to the inlet region for Richardson numbers of 5, 9, 14, 28, and 46, respectively. The three elevations (levels 1–3) shown in Figs. 6*a*–6*e* are at 12.5, 26, and 40 cm from the inlet (top of the tank). It can be seen that the addition of the perforated extension (perforated inlet with solid center) results in an improvement in stratification in the tank; the improvement varies depending on the Richardson number. Significant improvement is observed at a Richardson number of 5 (see Fig. 6*a*). As Richardson number increases beyond 9 (see Figs. 6*b*–6*e*), the difference in performance of the two inlets becomes insignificant, especially at elevations past 40 cm (1.3 ft) from the inlet (level 3). Based on these results, a limiting value of Richardson number of 9 may be deduced.

The results described in the foregoing agree well with the previous results of Refs. [4] and [5] concerning the existence of a limiting Richardson number, above which the effect of the inlet geometry on stratification in a thermal storage tank vanishes. However, the number deduced from the present study differs from those previously obtained. This should be expected for the following reasons.

1. The result of Ref. [5] was based on one-point concentration measurements far from the inlet in fresh-saline water systems. Figures 6*b*–6*e* indicate that the difference in performance of the two inlet geometries used gets smaller at locations removed from the inlet region, especially for Richardson numbers greater than 5.

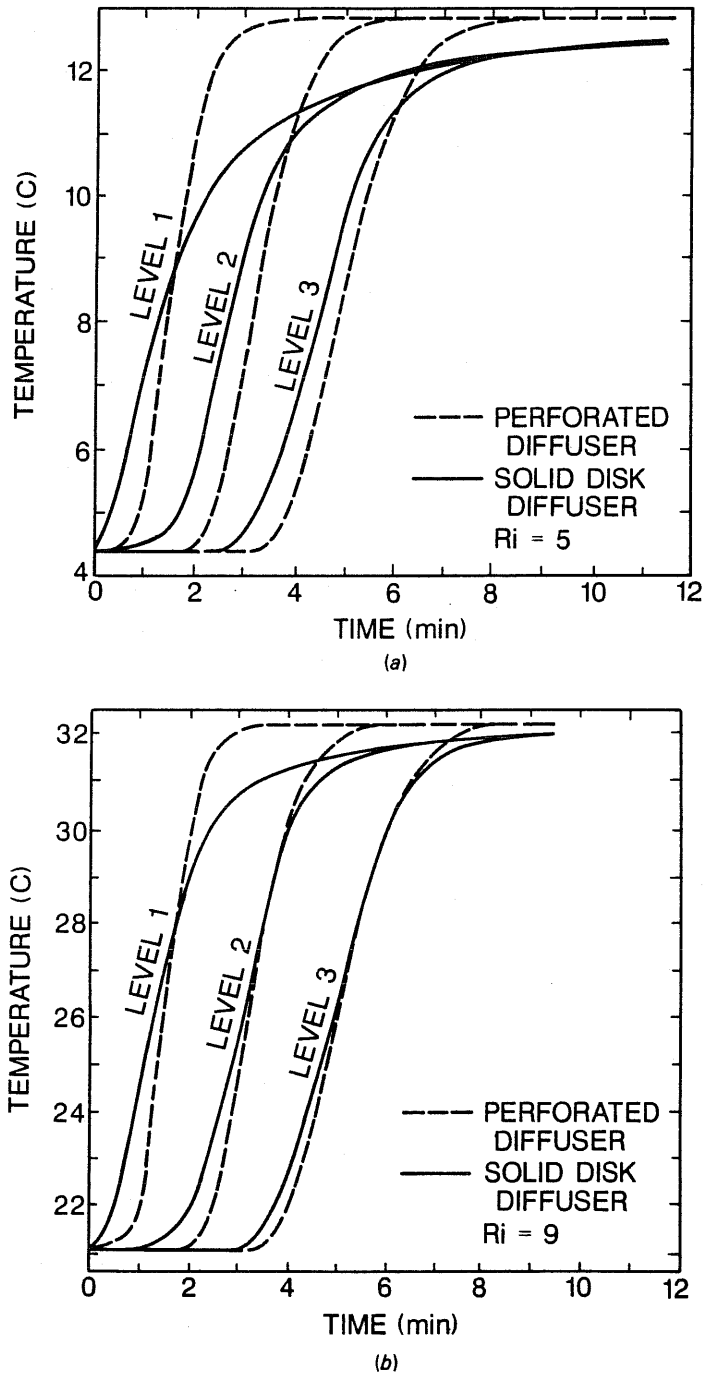

Fig. 6 Comparison of the predicted temperature profiles using SOUDS for two different inlet configurations and different Richardson numbers. (*a*) Ri = 5; (*b*) Ri = 9.

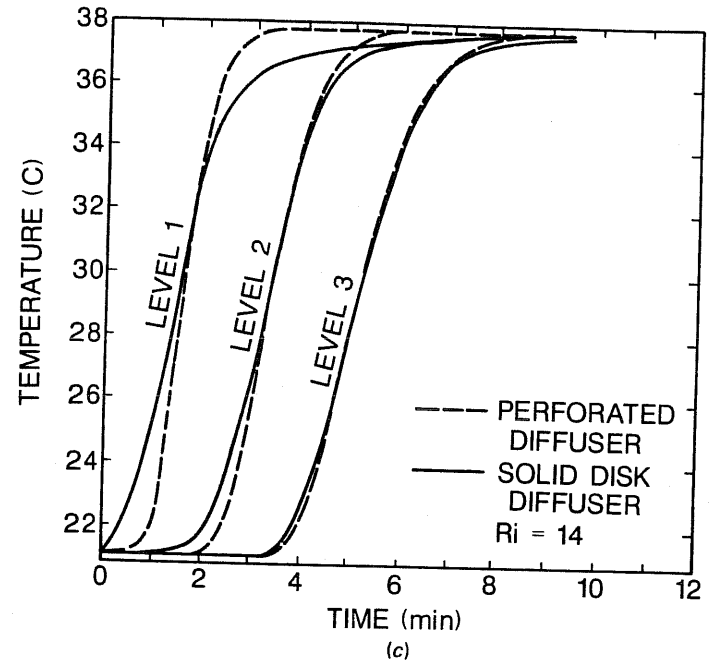

(c)

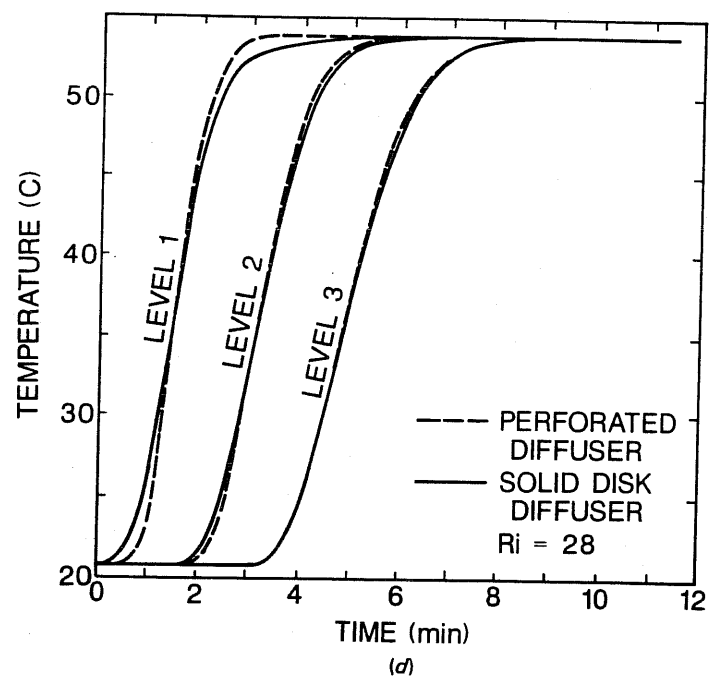

(d)

Fig. 6 (*Continued*). Comparison of the predicted temperature profiles using SOUDS for two different inlet configurations and different Richardson numbers. (*c*) Ri = 14; (*d*) Ri = 28.

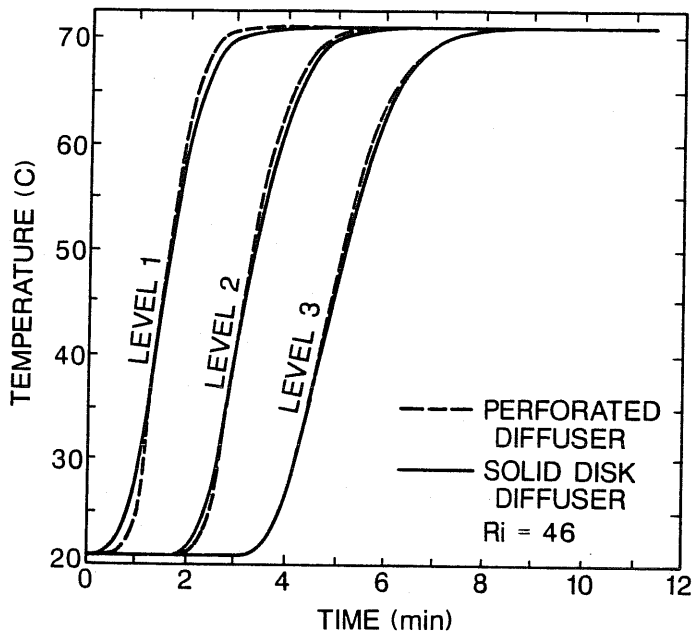

(e)

Fig. 6 (*Continued*). Comparison of the predicted temperature profiles using SOUDS for two different inlet configurations and different Richardson numbers. (*e*) Ri = 46.

2. The result of Ref. [4] was based on mixing correlations obtained through temperature measurements with hot-cold water systems. The measurements away from the inlet were used in obtaining the correlations.

Based on the results described in the foregoing, it may be stated that inlet geometry has a significant effect on stratification for Ri $\leq$ 5, a moderate effect for 5 $<$ Ri $\leq$ 9, and a negligible effect for Ri $>$ 10.

SUMMARY AND CONCLUSIONS

In this study a finite difference computer code incorporating the first- and second-order upstream difference schemes has been developed. The code, which also incorporated perforated and solid baffles and a wide range of boundary conditions, was applied to mixed convection flow in stratified thermal storage. It was shown that the second-order upstream difference scheme (SOUDS) is superior to the conventional upstream difference scheme or its derivative, the weighted upstream difference scheme (WUDS), since it produces less numerical diffusion and thus is more accurate. Therefore the effect of inlet geometry on stratification attainable was investigated using SOUDS. The results show that inlet geometry has a negligible effect on stratification for Richardson numbers above 10. This criterion is a significant contribution to the design of stratified thermal storage in solar energy applications.

REFERENCES

1. K. Y. Huh, M. W. Golay, and V. P. Manno, A Method for Reduction of Numerical Diffusion in the Donor Cell Treatment of Convection, *J. Comput. Phys.*, vol. 63, pp. 201–221, 1986.
2. Y. H. Zurigat and A. J. Ghajar, Comparative Study of Weighted Upwind and Second-Order Upwind Difference Schemes, *Numer. Heat Transfer, Part B*, vol. 18, no. 1, pp. 61–80, 1990.
3. Y. H. Zurigat, K. J. Maloney, and A. J. Ghajar, A Comparison Study of One-Dimensional Models for Stratified Thermal Storage Tanks, *J. Solar Energy Eng.*, vol. 111, no. 3, pp. 204–210, 1989.
4. Y. H. Zurigat, P. R. Liche, and A. J. Ghajar, Influence of Inlet Geometry on Mixing in Thermocline Thermal Energy Storage, *Int. J. Heat Mass Transfer*, 1990 (in press).
5. Y. H. Zurigat, A. J. Ghajar, and P. M. Moretti, Stratified Thermal Energy Storage Tank Inlet Mixing Characterization, *Appl. Energy*, vol. 30, pp. 99–111, 1988.
6. W. T. Sha, E. I. H. Lin, R. C. Schmitt, K. V. Lin, J. R. Hull, J. J. Oras, Jr., and H. M. Domanus, COMMIX-SA-1: A Three-Dimensional Thermohydrodynamic Computer Program for Solar Applications, Report ANL-80-8, Argonne National Laboratory, Argonne, Ill., 1980.
7. A. R. Sharif and A. A. Busnaina, Assessment of Finite Difference Approximations for the Advection Terms in the Simulation of Practical Flow Problems, *J. Comput. Phys.*, vol. 74, pp. 143–176, 1988.
8. Y. H. Zurigat, An Experimental and Analytical Examination of Stratified Thermal Storage, Ph.D. thesis, Oklahoma State University, Stillwater, Okla., 1988.
9. Engineering Sciences Data Unit Ltd., Engineering Sciences Data Item 72010, Pressure Losses Across Perforated Plates, Orifice Plates and Cylindrical Tube Orifices in Ducts, England, 1972.
10. B. Carnahan, H. A. Luther, and J. O. Wilkes, *Applied Numerical Methods*, John Wiley, New York, 1969.
11. C. W. Hirt, B. D. Nichols, and N. C. Romero, SOLA—A Numerical Solution Algorithm for Transient Fluid Flows, Report LA-5852, Los Alamos Scientific Laboratory, Los Alamos, N.M., April 1975.

Received 13 April 1990
Accepted 1 June 1990